Supporting Information for:

Electrochemical Ruthenium-Catalyzed C–H Activation in Water Through Heterogenization of a Molecular Catalyst

Jan Bühler,[a] Jonas Zurflüh,[a] Sebastian Siol,[b] Olivier Blacque,[a] Laurent Sévery*[a] and S. David Tilley*[a]

[a.] Department of Chemistry, University of Zurich, Winterthurerstrasse 190, 8057 Zurich, Switzerland. E-mail:
[b.] Empa – Swiss Federal Laboratories for Materials Science and Technology, Überlandstrasse 129, 8600 Dübendorf, Switzerland.

Contents

General information and instrumentation

Unless otherwise stated, all chemicals were of reagent grade or higher, obtained from commercial sources and used without further purification. Indium tin oxide (ITO) particles and proprietary nanopowder dispersant were purchased from *US Research Nanomaterials Inc.*, Houston, TX, USA. Fluorine doped tin oxide (FTO) glass slides were *Pilkington NSG TEC 15* (2.2 mm, 12–15 Ω/sq). Solvents for reactions were of p.a. grade; H_2O was ultrapure from a *Milli-Q® Direct 8* water purification system. D_2O was purchased from *Cambridge Isotope Laboratories, Inc.* (UK). **^{1}H and ^{13}C NMR** spectra were recorded on a *Bruker AV2-400* (400 MHz) in deuterated solvents at 300 K. Chemical shifts (δ) in ppm relative to residual solvent resonances (D_2O ^{1}H: δ 4.79; CD_3OD ^{1}H: δ 3.31; $CDCl_3$ ^{1}H: δ 7.26). Signal assignment are based on 2D experiments (COSY). **UV-Vis** spectra were recorded on a *Shimadzu UV-3600 Plus* spectrophotometer. **FT-IR** spectra were recorded with a *SpectrumTwo* FT-IR Spectrometer equipped with a *Specac Golden Gate*. **High-resolution electrospray mass** spectra (HR-ESI-MS) were recorded on a *timsTOF Pro TIMS-QTOF-MS* instrument (*Bruker Daltonics* GmbH, Bremen, Germany). The samples were dissolved in MeOH at a concentration of ca. 50 μg mL^{-1} and analyzed via continuous flow injection (2 μL min^{-1}). The mass spectrometer was operated in the positive or negative electrospray ionization mode at 4'000 V (−4'000 V) capillary voltage and −500 V (500 V) endplate offset with a N_2 nebulizer pressure of 0.4 bar and a dry gas flow of 4 L min^{-1} at 180 °C. Mass spectra were acquired in a mass range from m/z 50 to 2'000 at ca. 20'000 resolution (m/z 622) and at 1.0 Hz rate. The mass analyzer was calibrated between m/z 118 and 2'721 using an *Agilent* ESI-L low concentration tuning mix solution (*Agilent*, USA) at a resolution of 20'000 giving a mass accuracy below 2 ppm. All solvent used were purchased in best LC-MS quality. **Scanning electron microscopy** (SEM) images were obtained from a *Zeiss Supra* 50 VP instrument. Samples were scored and cleaved using a glass-breaking plier, ensuring pristine edges where the measurements were performed. The pieces were attached to aluminum pins with carbon stickers and electrically connected on the edge using silver paste or carbon paste. Images shown below were collected using the *Inlens* detector, with an electron acceleration voltage of 5 kV. **X-ray photoelectron spectroscopy** (XPS) was conducted on selected samples using a *Physical Electronics* (PHI) Quantum 2000 X-ray photoelectron spectrometer featuring monochromatic Al-Kα radiation, generated from an electron beam operated at 15 kV and 28.76 W. The linearity of the energy scale of the instrument was calibrated using Au and Cu reference samples. The C–C component of adventitious carbon was further referenced to 284.8 eV. The analysis was conducted at $8 \cdot 10^{-9}$ mbar, with an electron take off angle of 45° and a pass energy of 23.50 eV for all samples. Charge compensation during the measurement was achieved using a low energy electron source. Due to the overlapping core level spectra of the C 1s and Ru 3d emission the spectra were fitted to deconvolute the respective contributions after *Shirley* background subtraction. The C 1s emission was fit using 3 GL(30) components corresponding to C–C; C–O–C, C–O–H, C–Cl as well as C=O at binding energies of 284.8, 286 and 288.5 eV, respectively. The Ru 3d peak was fitted using an asymmetric peak shape (LF(0.8,1.25,500,180)) and a constant doublet splitting of D = 4.2 eV resulting in binding energies of 280.7 and 284.9 eV for the Ru 3d 5/2 and 3d 3/2, respectively.

Syntheses

[Ru(tpy)Cl_3] (1)
Prepared according to literature procedure.[1]

FT-IR (ν_{max}/cm^{-1}): 3062 (aromatic C–H), 1594 (C=N), 1444 (C=C), 779 (aromatic C–H) (in agreement with previously reported data[1]).

4-Phosphonopyrid-2-ylcarboxylic acid (pic-PO_3H_2) (2)
Prepared according to literature procedure.[2]

^{1}H NMR (D_2O, 400 MHz): δ 8.83 (1 H, dd, *J* = 5.5, 2.8 Hz), 8.60 (1 H, d, *J* = 11.4 Hz), 8.33 (1 H, dd, *J* = 11.0, 5.7 Hz) (in agreement with previously reported data[2]).

[Ru(tpy)(pic-PO_3H_2)Cl] (3)
To a dark solution of [Ru(tpy)Cl_3] (220 mg, 0.50 mol, 1 eq.), LiCl (130 mg, 3.02 mmol, 6 eq.) and NEt_3 (140 µL, 1.00 mmol, 2 eq.) in EtOH/H_2O (3:1, 20 mL) was added 4-phosphonopyrid-2-ylcarboxylic acid (101 mg, 0.50 mmol, 1 eq.). The mixture was heated to 78 °C for 3 h whereupon a color change to deep red was observed. The reaction mixture was filtered hot through a glass filter frit, condensed to about 2 mL and cooled to 4 °C for 24 h to initiate crystallization. The dark purple crystals were collected on a glass filter frit and washed with an ice-cold aqueous solution of HCl (3 M, 3 × 5 mL), acetone (3 × 10 mL) and Et_2O (3 × 10 mL) to afford [Ru(tpy)(pic-PO_3H_2)Cl] (**3,** 182 mg, 0.32 mmol, 64%).

^{1}H NMR (D_2O, 400 MHz): δ 8.55 (2H, d, *J* = 5.2 Hz, H1), 8.48 (2 H, d, *J* = 8.1 Hz, H5), 8.43 (2 H, d, *J* = 8.1 Hz, H4), 8.10 (1 H, d, *J* = 11.7 Hz, H7), 8.05–8.00 (2 H, m, H3 and H6), 7.61 (1 H, t, *J* = 6.2 Hz, H2), 7.14–7.07 (2 H, m, H8 and H9).
^{13}C-NMR (D_2O, 500 MHz): δ 174.7 (Ce), 161.1 (Ca), 159.2 (Cb), 154.1 (Cd), 152.9 (C9), 151.8 (C1), 142.8 (Cc), 138.0 (C3), 133.1 (C6), 128.2 (C8), 127.8 (C2), 127.3 (C7), 123.5 (C4), 122.65 (C5).
HRMS (ESI) m/z: $[M-H]^-$ calcd. for $C_{21}H_{15}ClN_4O_5PRu$ 570.9518; found: 570.9518.

[Ru(tpy)(pic-PO_3Et_2)Cl]
To a dark solution of [Ru(tpy)Cl_3] (30 mg, 68 µmol, 1 eq.), LiCl (18 mg, 425 µmol, 6 eq.) and NEt_3 (20 µL, 142 µmol, 2 eq.) in EtOH/H_2O (3:1, 4 mL) was added ethyl 4-diethoxyphosphorylpyrid-2-ylcarboxylate (20 mg, 69 µmol, 1 eq.). The mixture was heated to 78 °C for 3 h whereupon a color change to deep red was observed. The reaction mixture was filtered hot through a glass filter frit, condensed to about 0.5 mL and cooled to 4 °C for 24 h to initiate precipitation. The dark purple powder was collected on a glass filter frit and washed with acetone and Et_2O to afford [Ru(tpy)(pic-PO_3Et_2)Cl] (25 mg, 40 µmol, 58%).

^{1}H NMR (CD_3OD, 400 MHz): δ 10.21 (1 H, t, *J* = 4.9 Hz), 8.53 (2 H, d, *J* = 8.1 Hz), 8.49 (2 H, dd, *J* = 8.1, 3.2 Hz), 8.41 (1 H, dd, *J* = 13.0, 1.1 Hz), 8.05 (1 H, ddd, *J* = 12.8, 5.6, 1.7 Hz,), 8.02 (2 H, d, *J* = 5.5 Hz), 7.98–7.87 (3 H, m), 7.45 (2 H, td, *J* = 6.5, 1.0 Hz), 4.37 (4 H, m), 1.48 (6 H, t, *J* = 7.05 Hz).
HRMS (ESI) m/z: $[M-H]^-$ calcd. for $C_{25}H_{24}ClN_4O_5PRu$ 628.02163; found: 628.02109.

[Fe(tpy)(pic-PO_3H_2)Cl]
To a purple solution of $FeCl_2$ (25 mg, 0.20 mmol, 1 eq.) and terpyridine (46 mg, 0.20 mmol, 1 eq.) in degassed MeOH (4 mL) was dropwise added a solution of 4-phosphonopyrid-2-ylcarboxylic acid (1 mg, 0.20 mmol, 1 eq.) and NaOH (24 mg, 0.60 mmol, 3 eq.) in degassed MeOH/H_2O (2:1, 12 mL). The mixture was heated to 78 °C for 5 h and filtered hot through a glass filter frit, condensed to about 2 mL and cooled to 4 °C for 24 h to initiate precipitation. The dark purple powder was collected on a glass filter frit and washed with an aqueous solution of HCl (3 M), acetone and Et_2O to afford [Fe(tpy)(pic-PO_3H_2)Cl] (62 mg, 0.12 mmol, 60%).

^{1}H NMR (D_2O, 400 MHz): δ 8.70 (2 H, d, *J* = 7.5 Hz), 8.61 (1 H, t, *J* = 7.3 Hz), 8.52 (1 H, t, *J* = 4.1 Hz), 8.48 (2 H, d, *J* = 7.9 Hz), 8.13 (1 H, d, *J* = 11.6 Hz), 8.03 (2 H, t, *J* = 7.4 Hz), 7.77 (1 H, ddd, *J* = 11.3, 5.1, 1.2 Hz), 7.68 (2 H, br. s), 7.26 (2 H, t, *J* = 6.1 Hz).
HRMS (ESI) m/z: $[M-H]^-$ calcd. for $C_{21}H_{15}ClFeN_4O_5P$ 524.9818; found: 524.9817.

Electrode Preparation

Preparation of the ITO Spin-Coating Suspension

ITO particles (18 nm, 99.99%, 2.0 g) were sonicated in EtOH (10 mL) for 20 min. A solution of ethyl cellulose (200 mg), alcohol surfactant (proprietary nanopowder dispersant, 225 mg), and terpineol (5.0 g) in ethanol (5 mL) was added and the resulting suspension was sonicated for 5 min. The volatiles were removed by rotary evaporation to form a viscous blue paste. Dilution of the paste with EtOH (1:4) yielded the suspension used for spin-coating.

Preparation of *meso*-ITO coated FTO Electrodes

FTO glass slides (2.5×1.2 cm) were cleaned by subsequent sonication in acetone, H_2O containing alkaline detergent (*Deconex 11 Universal*), H_2O and EtOH for 10 min each. A portion of the substrate was covered with thermostable tape (*Kapton*). The exposed area (1.4×1.2 cm; 1.66 cm^2) was treated with freshly sonicated ITO spin-coating suspension (30 µL) and spin-coated (2000 rpm, 500 rpm s^{-1}, 20 s). The solvent was evaporated on a hot plate at 120 °C for 10 min. The spin coating was repeated twice (40 and 50 µL of ITO suspension). The thermostable tape was removed and the electrode was sintered on a hot plate at 450 °C in air for 30 min (20 min ramp time).

Catalyst Immobilization

Freshly prepared *meso*-ITO electrodes were soaked in a solution of [Ru(tpy)(pic-PO_3H_2)Cl] (**3**) in MeOH (1 mM, 10 mL) for 60 min. The soaked electrodes were rinsed with MeOH, dried under a stream of N_2, heated on a hot plate to 100 °C for 10 min, and then allowed to cool naturally to room temperature.

Determination of Catalyst Loading

UV-Vis spectra of solutions of [Ru(tpy)(pic-PO_3H_2)Cl] (3, 17, 51 and 102 mM) in aqueous KOH (1 M) were recorded for the determination of an external calibration curve (Figure S5).

[Ru(tpy)(pic-PO_3H_2)Cl] (**3**) was immobilized on *meso*-ITO electrodes (as described above). The electrodes were then soaked in an aqueous solution of KOH (1 M, 5 mL) for 5 min to completely desorb the catalyst. ITO particles were removed by filtration of the solution through a syringe filter before UV-Vis spectra were recorded.
The catalyst loading was calculated according to the following formulas:

(1) $C = \frac{(m-A)}{b}$

The concentration (C) of the desorbed catalyst is calculated from the slope (m) and axial intercept (b) of the calibration curve (Figure S5b), where A is the absorbance of the measured sample. This is calculated for three different wavelengths (373, 414 and 512 nm) and the average is taken.

(2) $Catalyst\ Loading = \frac{C*V}{A_E}$

The catalyst loading is calculated from the concentration (C) multiplied by the volume (V) of the desorption solution divided by the area of the electrode (A_E).

Electrochemistry

Standard Conditions

Cyclic voltammetry and chronoamperometry experiments were performed on a *Bio-Logic SP-50* potentiostat in aqueous Na_2SO_4 (8 mL, 0.1 M, pH 2.4). Teflon (PTFE) tape was used to control the exposed surface area of the working electrode (Exposed geometric area was set to: 1.4 cm · 1.2 cm = 1.68 cm^2). Freshly flamed Pt wire was used as counter electrode and Ag/AgCl (sat. KCl) as reference electrode. Solutions used for chronoamperometry experiments were stirred at 500 rpm with a magnetic stir bar. Unless stated otherwise, voltages are reported vs. the normal hydrogen electrode (NHE) by converting the measured potentials (vs. Ag/AgCl) using the following equation: $E_{NHE} = E_{Ag\ /\ AgCl} + 0.199\ V$.

Determination of Product Formation

Reaction mixtures of chronoamperometry experiments were extracted with $CDCl_3$ (1 mL) and the organic phase was dried over anhydrous $MgSO_4$ (1,4-cyclohexadiene, benzyl alcohol, toluene and n-butanol) or the solvent was evaporated and the residue dissolved in $(CD_3)_2SO$ (1 mL)(S_2-fluorene). The qualitative and quantitative conversion of the starting materials was determined by ^1H NMR.

Homogeneous TOF Analysis

Equations used to calculate TOF:[3,4]

(3) $i_c = nFAC_P^0\sqrt{Dk_{obs}}$

The kinetic parameter k_{obs} is derived from equation 3, where the catalytic plateau current i_c can be determined using n, which represents the number of transferred electrons from the electrode to the catalyst, the faraday constant F, the electrode surface area A, the concentration of catalyst C_P^0 and the diffusion coefficient P.

(4) $i_p = 0.4463nFAC_P^0\sqrt{\frac{nFDv}{RT}}$

Equation 4 (Randles-Sevcik equation) describes the dependence of the peak current i_p on the scan rate v for a reversible redox process (in this case the Ru^{III}/Ru^{IV} redox event). Combining these two yields equation 5, where D, A and C_P^0 no longer have to be measured independently:

(5) $\frac{i_c}{i_p} = \frac{\sqrt{\left(\frac{RT}{nF}\right)}}{0.4463}\sqrt{k_{obs}}\sqrt{\frac{1}{v}}$

In our case, T = 298, n = 2, which leads to the expression:

(6) $\frac{i_c}{i_p} = 0.254\sqrt{k_{obs}}\sqrt{\frac{1}{v}}$

The resulting equation 6 enables the calculation of $\sqrt{k_{obs}}$ as the slope of the i_c/i_p ratios at different scan speeds versus the square root of $1/v$ and be converted into k_{obs} according to the relationship $(Slope/0.254)^2 = k_{obs}$ and found to be 0.052 s^{-1} for 2.4 mM, 0.236 s^{-1} for 4.8 mM and 0.493 s^{-1} for 9.6 mM substrate concentration. The analysis was restricted to where the i_c/i_p and thus only the 3 lowest substrate concentrations were used for the determination (see Figure S3). The kinetic parameter k_{cat} was estimated by using the relation $k_{obs}=k_{cat}\cdot C_{BnOH}^0$ and found to be 41 ± 14 M^{-1} s^{-1}.

An expected value of 18.0 ± 0.8 M^{-1} s^{-1} was obtained for the kinetic parameter k_{cat} from the heterogeneous experiment by applying the following relation:

(7) $k_{cat} = \frac{i}{Catalyst\ loading * A * n * F * C_{BnOH}^0}$

Where the current (i) was 0.9 mA (after 10 s of chronoamperometry), the surface loading 15.4 ± 0.7 nmol cm^{-2}, the electrode area (A) 1.68 cm^2 and the number of electrons per reaction (n) 2.

Pourbaix Diagrams

Experimental Conditions

Cyclic voltammetry measurements for the construction of the Pourbaix diagrams were performed in Britton–Robinson buffer (0.1 M) and the pH was adjusted by addition of an aqueous solution of NaOH (5 M). Data were collected in the pH range 2.0–5.0 and the potential range of 0.20–1.65 V vs. NHE with a scan speed of 100 mV s^{-1}. Redox potentials for the Ru^{II}/Ru^{III}, Ru^{III}/Ru^{IV} and L–H/$L^{\cdot}$ redox pairs were extracted from CV data by taking the mean of the oxidative and reductive waves. Representative CV spectra for $[Ru(tpy)(pic\text{-}PO_3H_2)(H_2O)]^+(Cl)^-$ in solution and immobilised on a *meso*-ITO electrode are shown in Figure S16.

Calculation of the Bond Dissociation Energy

The bond dissociation energy (BDE) of the O–H bond in $[Ru^{III}(tpy)(pic\text{-}PO_3H_2)(OH)]^+$ can be calculated according to equation 8, where the pK_a and $E_{Ox}(A^-)$ are determined from the Pourbaix diagram of immobilised $[Ru(tpy)(pic\text{-}PO_3H_2)(H_2O)]^+(Cl)^-$ and C is a constant (55.8 kcal mol^{-1} in H_2O).[5,6]

(8) $$BDE = 1.37pK_a + 23.06E_{Ox}(A^-) + C$$

Additional figures

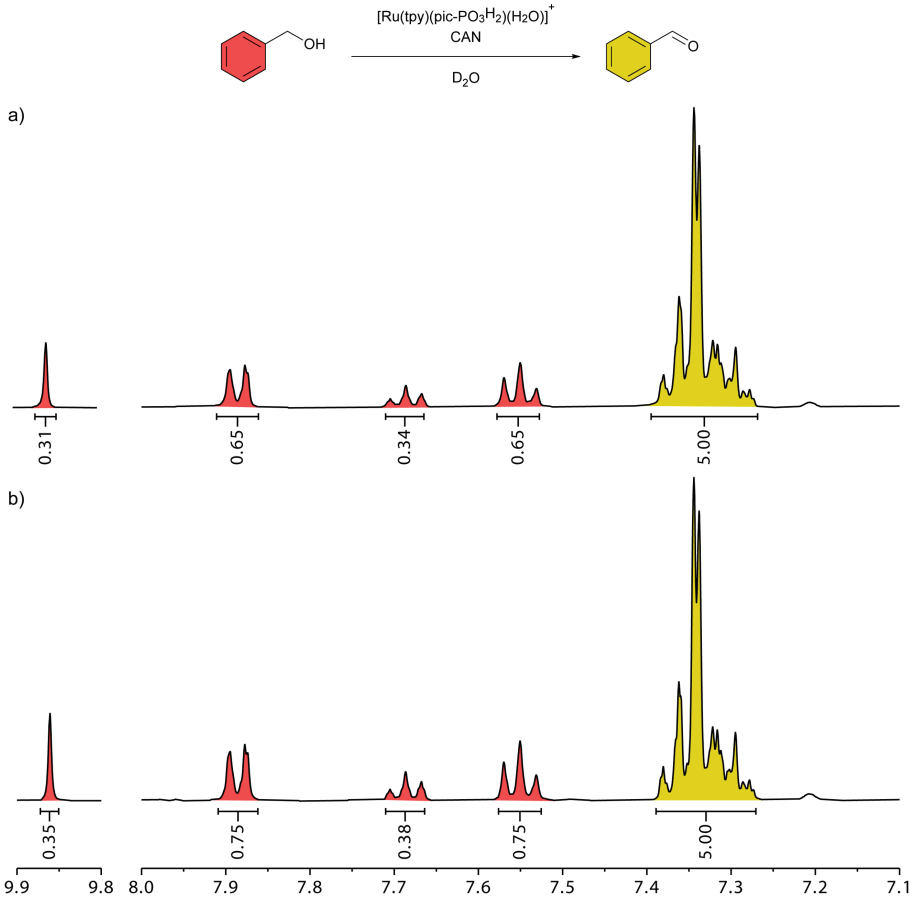

Fig. S1 Catalytic conversion of benzyl alcohol to benzaldehyde using $[Ru(tpy)(pic\text{-}PO_3H_2(H_2O)]^+$ and CAN. Conditions: $[Ru(tpy)(pic\text{-}PO_3H_2(H_2O)]^+$ (1 eq.), CAN (40 eq.) and benzyl alcohol (20 eq.) in D_2O (10 mL). a) After 1 h reaction time, 25% conversion corresponding to 4.9. b) After 2 h reaction time, 27% conversion corresponding to a TON of 5.4.

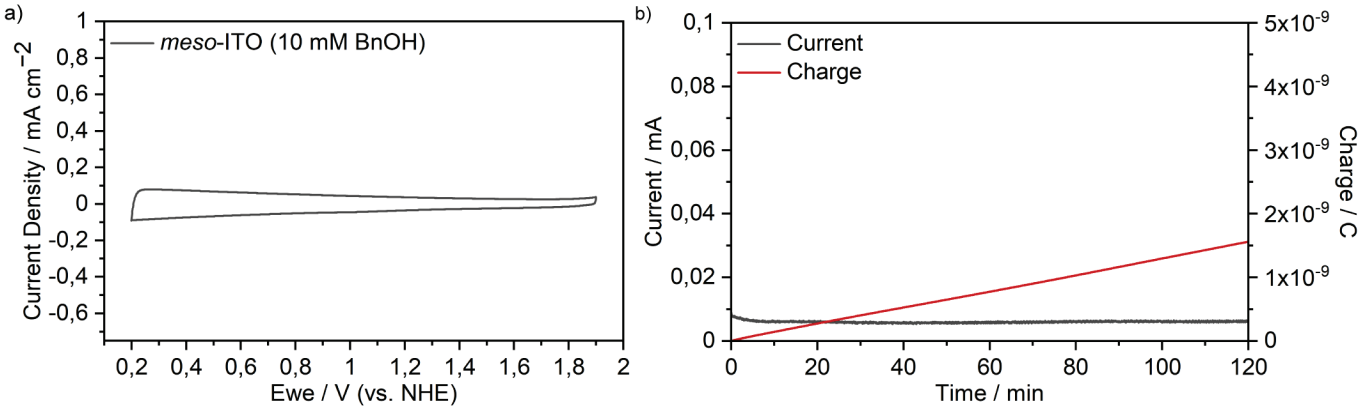

Fig. S2 a) Cyclic voltammogram of benzyl alcohol (10 mM) with a meso-ITO working electrode in aqueous Na_2SO_4 (0.1 M, pH 2.4) at 100 mV s^{-1}. b) Chronoamperometry of benzyl alcohol (10 mM) in aqueous Na_2SO_4 (0.1 M, pH 2.4) at 1.45 V vs. NHE.

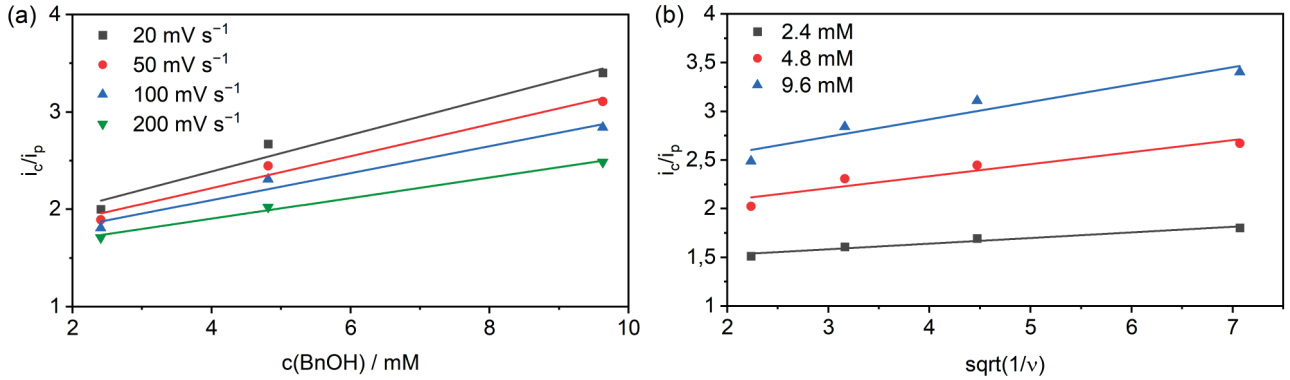

Fig. S3 (a) i_c/i_p values obtained at different scan speeds versus various concentrations of BnOH. i_c and i_p currents were obtained at 1.35 V vs. NHE in standard CV experiments with an FTO working electrode. (b) Plot of obtained i_c/i_p ratio versus the square root of the inverse of the scan speed for three substrate concentrations.

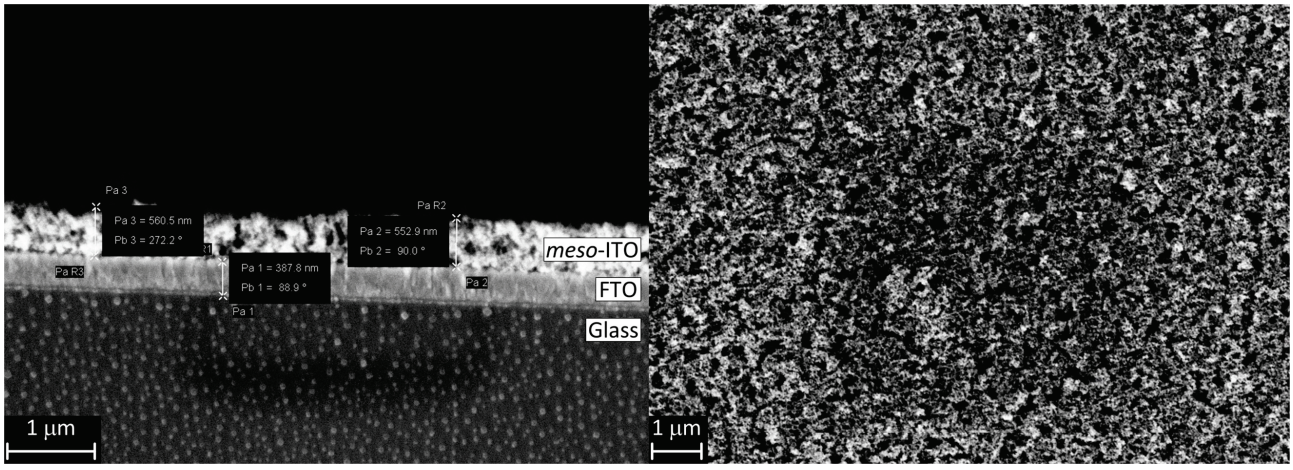

Fig. S4 SEM images of meso-ITO in cross-sectional (left) and top (right) view.

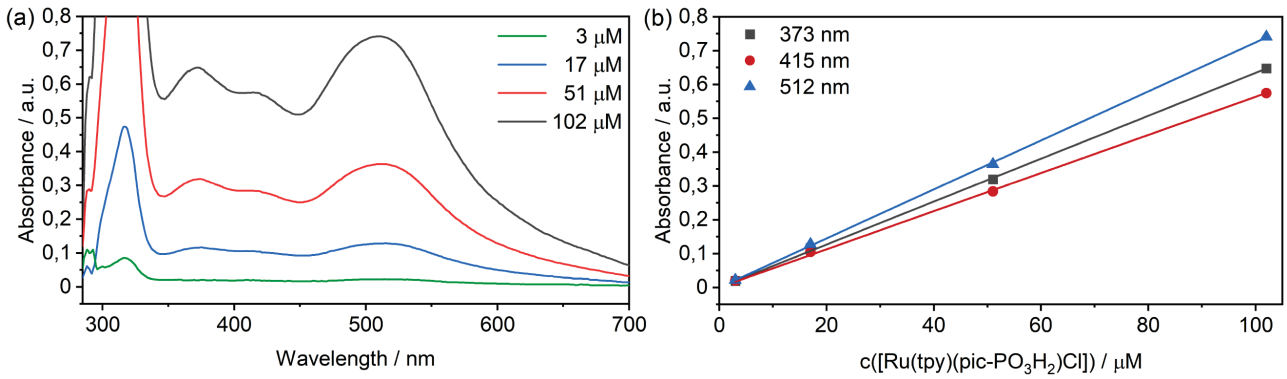

Fig. S5 (a) UV-Vis spectra at different concentrations of [Ru(tpy)(pic-PO_3H_2)Cl] (**3**) in aqueous KOH (1 M). (b) Derived calibration curves at 373 nm (slope: $7.25 \cdot 10^{-3}$ µmol^{-1}), 415 nm (slope: $5.64 \cdot 10^{-3}$ µmol^{-1}) and 512 nm (slope: $6.34 \cdot 10^{-3}$ µmol^{-1}).

Table S1. Calculation of the catalyst loading.

Measurement	1	2	3	Average
Absorbance (373 nm)	$3.6 \cdot 10^{-2}$	$3.7 \cdot 10^{-2}$	$3.3 \cdot 10^{-2}$	$3.5 \cdot 10^{-2}$
Absorbance (415 nm)	$3.4 \cdot 10^{-2}$	$3.4 \cdot 10^{-2}$	$3.1 \cdot 10^{-2}$	$3.3 \cdot 10^{-2}$
Absorbance (512 nm)	$3.4 \cdot 10^{-2}$	$3.5 \cdot 10^{-2}$	$3.1 \cdot 10^{-2}$	$3.3 \cdot 10^{-2}$
Catalyst concentration (µmol/L)	5.47	5.57	4.99	5.34 ± 0.25
Catalyst loading (nmol cm−2)	15.1	15.4	13.6	15.4 ± 0.7

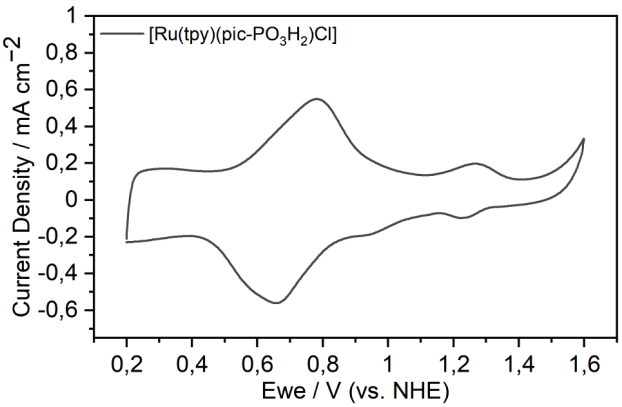

Fig. S6 Cyclic voltammogram of [Ru(tpy)(pic-PO_3H_2)Cl] immobilized on a meso-ITO electrode in aqueous Na_2SO_4 (0.1 M, pH 2.4) at 100 mV s^{-1}, cycled between 0.35 and 1.75 V.

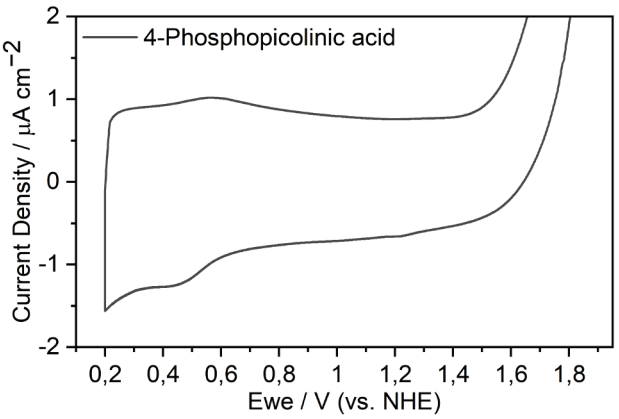

Fig. S7 Cyclic voltammogram of 4-phosphonopyrid-2-ylcarboxylic acid in aqueous Na_2SO_4 (0.1 M, pH 2.4) at 100 mV s^{-1}.

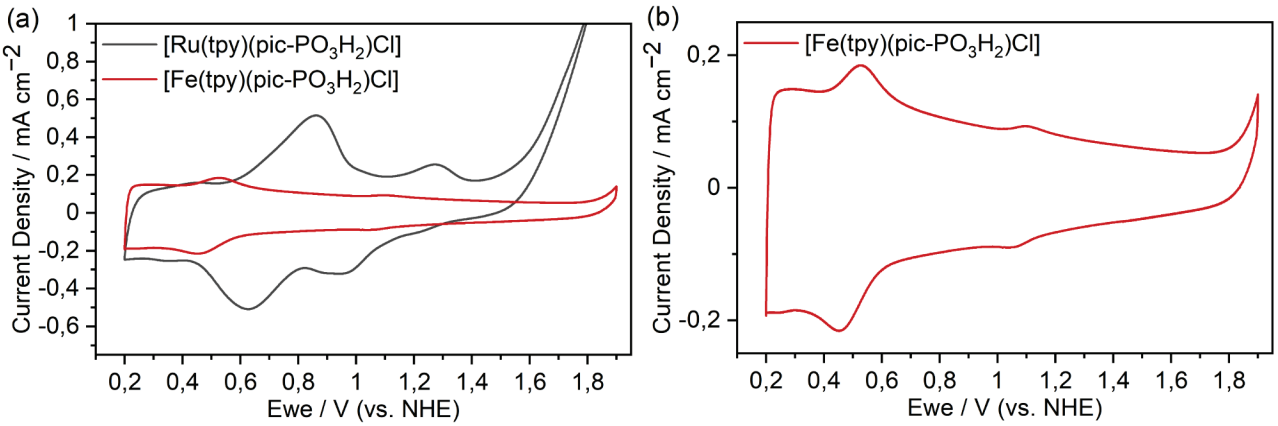

Fig. S8 (a) Cyclic voltammograms of [Ru(tpy)(pic-PO_3H_2)Cl] and [Fe(tpy)(pic-PO_3H_2)Cl] immobilized on a *meso*-ITO electrode in aqueous Na_2SO_4 (0.1 M, pH 2.4) at 100 mV s^{-1}. (b) Enhanced view of the cyclic voltammogram of [Fe(tpy)(pic-PO_3H_2)Cl].

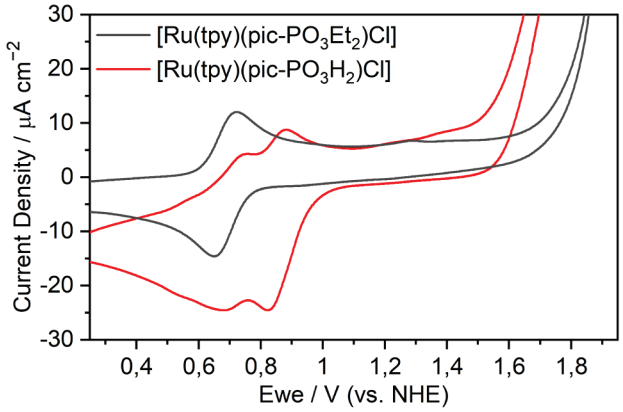

Fig. S9 Cyclic voltammograms of [Ru(tpy)(pic-PO_3H_2)Cl] and [Ru(tpy)(pic-PO_3Et_2)Cl] in aqueous Na_2SO_4 (0.1 M, pH 2.4) at 100 mV s^{-1}.

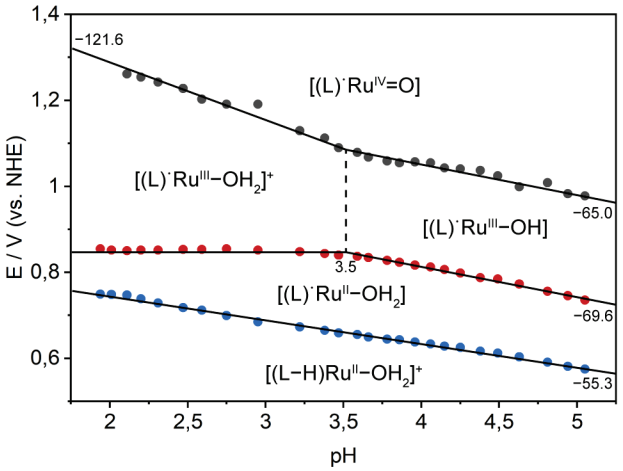

Fig. S10 Pourbaix diagram of [Ru(tpy)(pic-PO3H2)(H2O)]+[Cl]−(homogeneous solution) in the pH range of 2.0–5.0 (pKa value is denoted by the vertical dashed line, slopes are given in mV pH−1). Experimental conditions: Britton–Robinson buffer (0.1 M), pH was adjusted with an aqueous solution of NaOH (5 M).

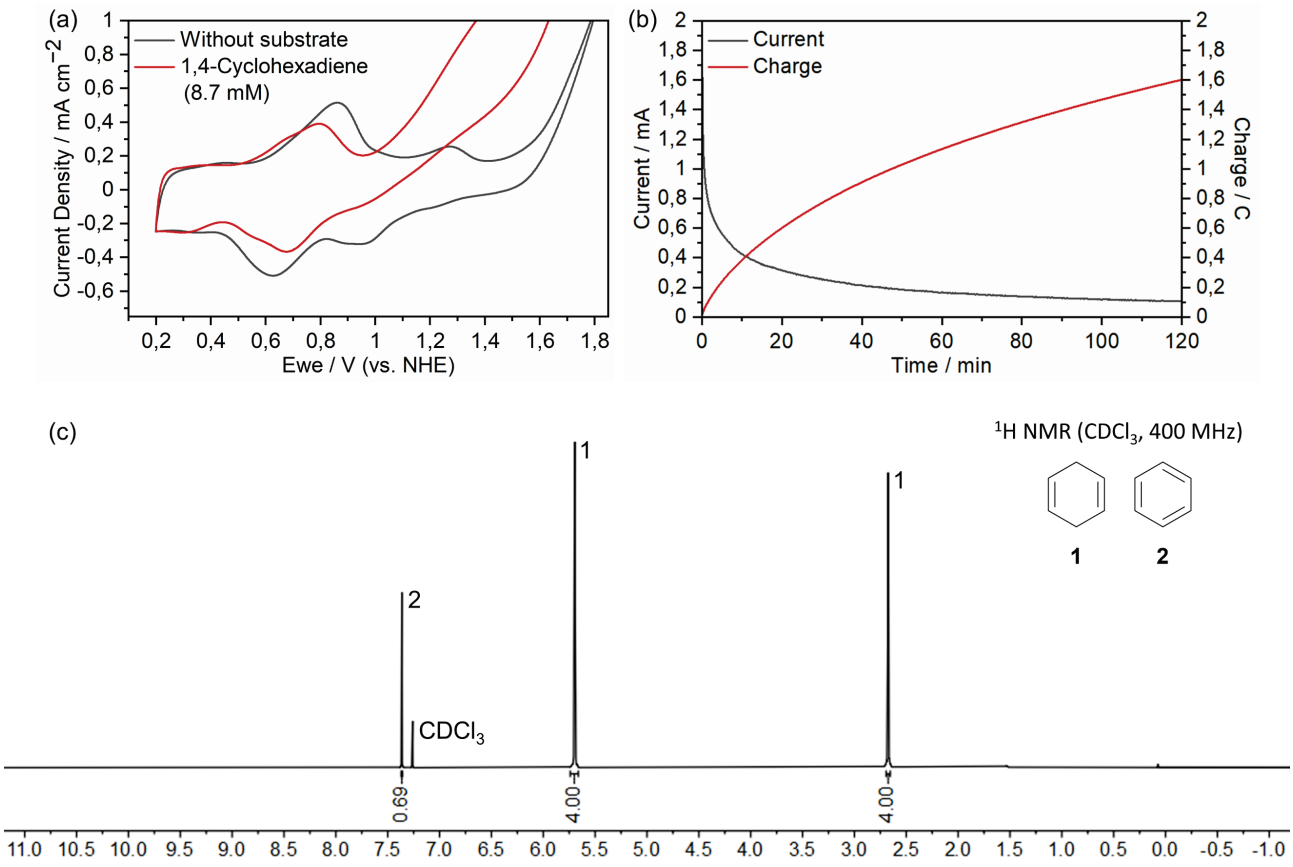

Fig. S11 (a) Cyclic voltammogram of [Ru(tpy)(pic-PO_3H_2)Cl] immobilized on a *meso*-ITO electrode in aqueous Na_2SO_4 (0.1 M, pH 2.4) and after addition of 1,4-cyclohexadiene (8.7 mM) at 100 mV s^{-1}. (b) Chronoamperometry of 1,4-cyclohexadiene in aqueous Na_2SO_4 (0.1 M, pH 2.4) at 1.45 V vs. NHE. (c) ^{1}H NMR of reaction solution after chronoamperometry in $CDCl_3$.

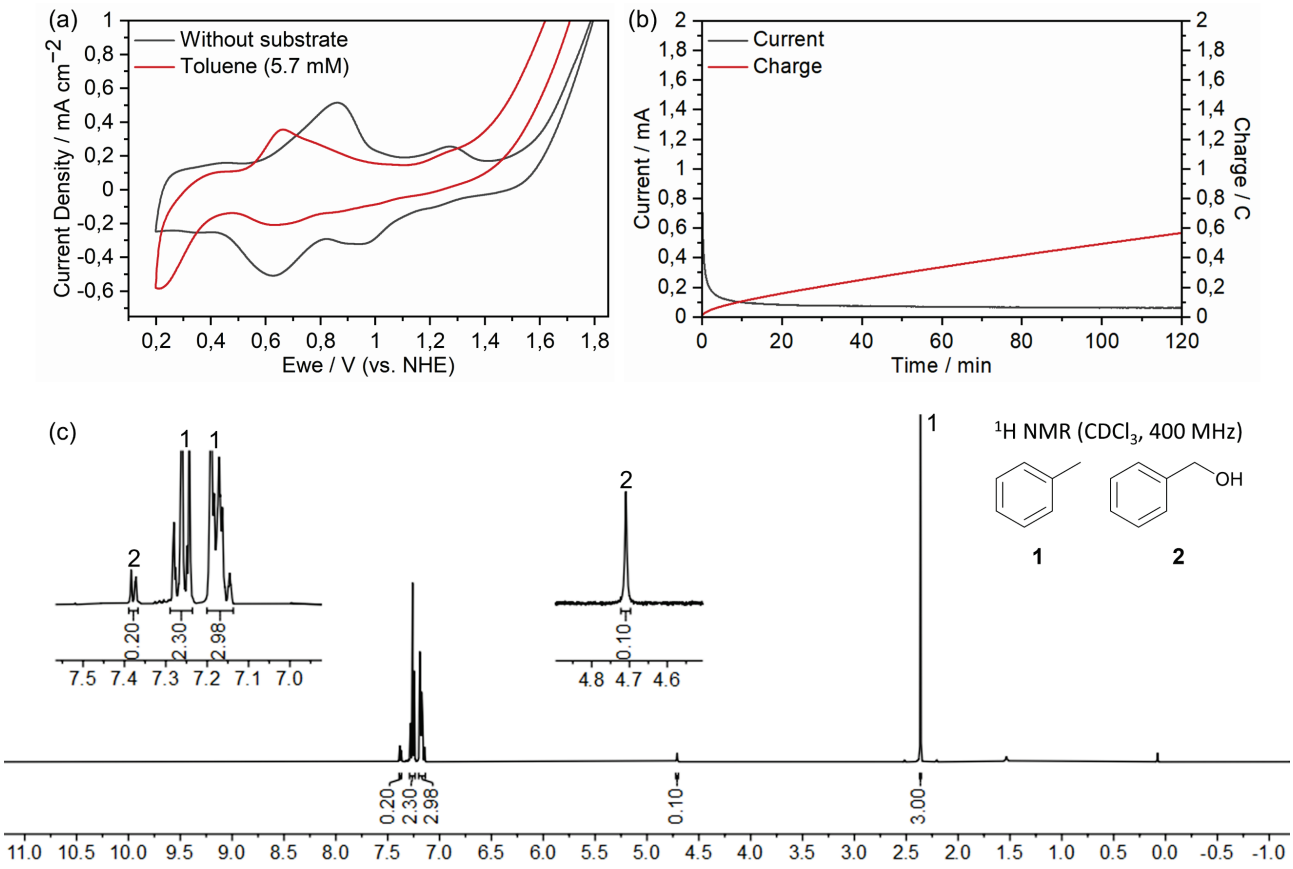

Fig. S12 (a) Cyclic voltammogram of [Ru(tpy)(pic-PO_3H_2)Cl] immobilized on a meso-ITO electrode in aqueous Na_2SO_4 (0.1 M, pH 2.4) and after addition of toluene (5.7 mM) at 100 mV s^{-1}. (b) Chronoamperometry of toluene in aqueous Na_2SO_4 (0.1 M, pH 2.4) at 1.45 V vs. NHE. (c) ^{1}H NMR of reaction solution after chronoamperometry in $CDCl_3$.

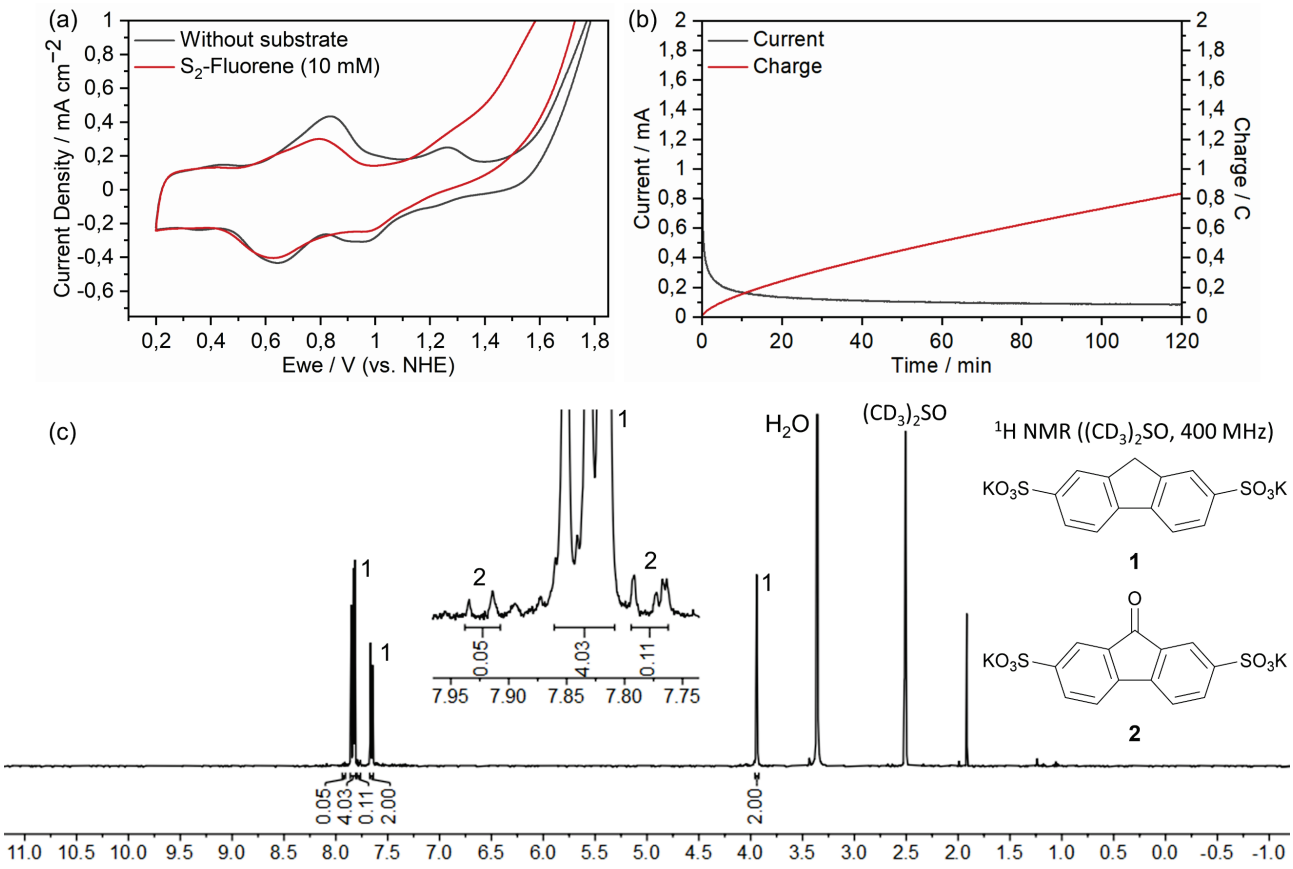

Fig. S13 (a) Cyclic voltammogram of [Ru(tpy)(pic-PO_3H_2)Cl] immobilized on a meso-ITO electrode in aqueous Na_2SO_4 (0.1 M, pH 2.4) and after addition of S_2-fluorene (10 mM) at 100 mV s^{-1}. (b) Chronoamperometry of S_2-fluorene in aqueous Na_2SO_4 (0.1 M, pH 2.4) at 1.45 V vs. NHE. (c) ^{1}H NMR of reaction solution after chronoamperometry in $CDCl_3$.

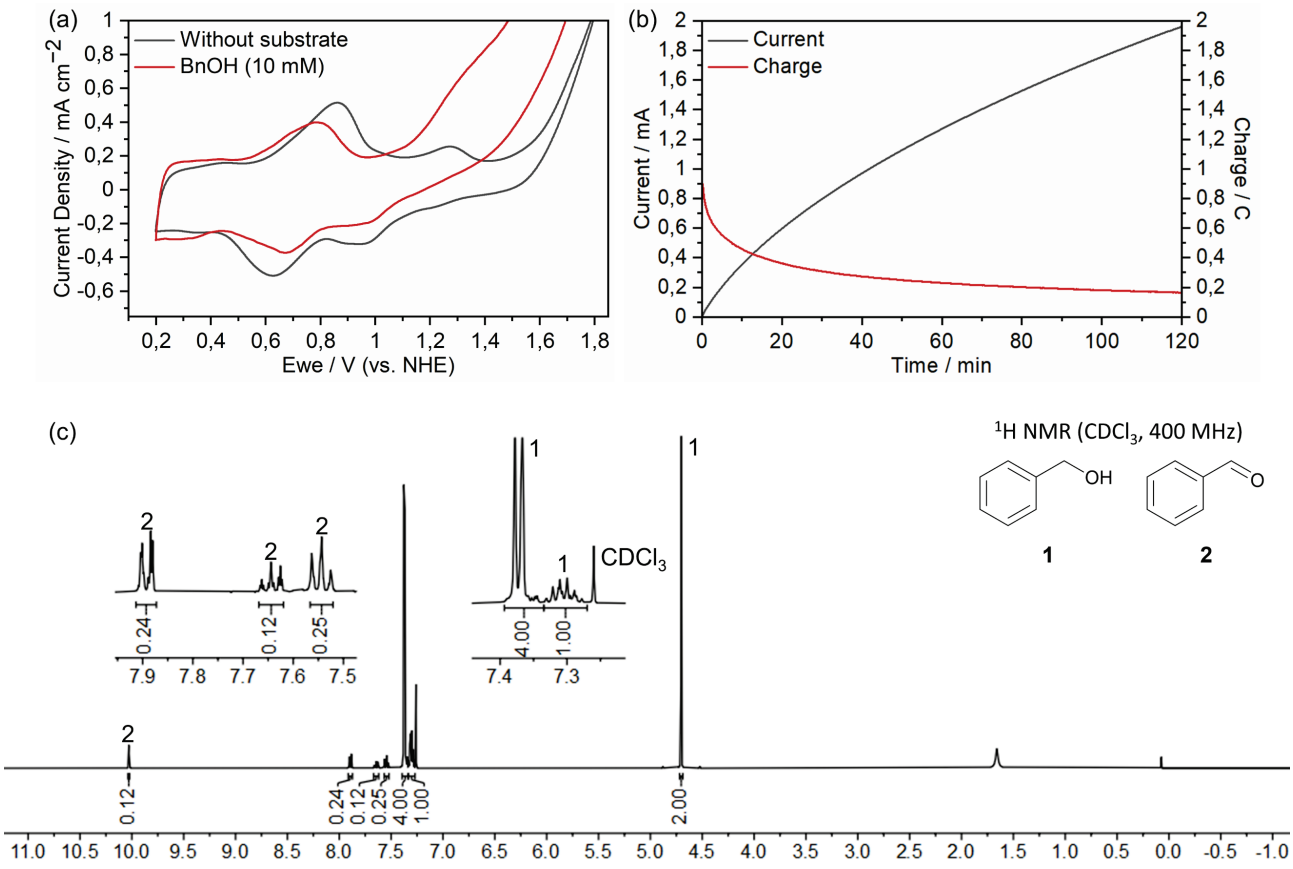

Fig. S14 Cyclic voltammogram of [Ru(tpy)(pic-PO_3H_2)Cl] immobilized on a meso-ITO electrode in aqueous Na_2SO_4 (0.1 M, pH 2.4) and after addition of benzyl alcohol (10 mM) at 100 mV s^{-1}. (b) Chronoamperometry of benzyl alcohol in aqueous Na_2SO_4 (0.1 M, pH 2.4) at 1.45 V vs. NHE. (c) ^{1}H NMR of reaction solution after chronoamperometry in $CDCl_3$.

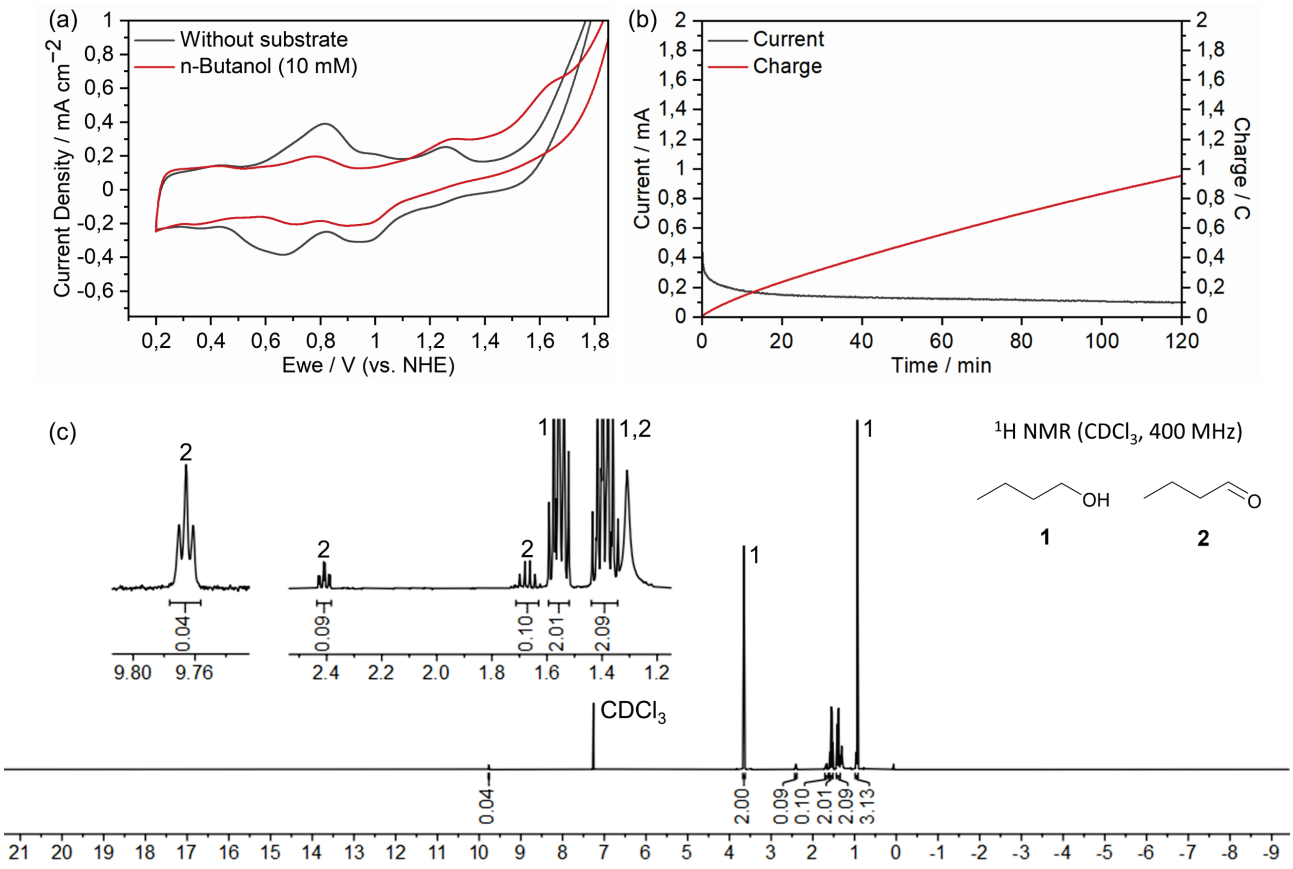

Fig. S15 (a) Cyclic voltammogram of [Ru(tpy)(pic-PO_3H_2)Cl] immobilized on a *meso*-ITO electrode in aqueous Na_2SO_4 (0.1 M, pH 2.4) and after addition of n-butanol (10 mM) at 100 mV s^{-1}. (b) Chronoamperometry of n-butanol in aqueous Na_2SO_4 (0.1 M, pH 2.4) at 1.45 V vs. NHE. (c) ^{1}H NMR of reaction solution after chronoamperometry in $CDCl_3$.

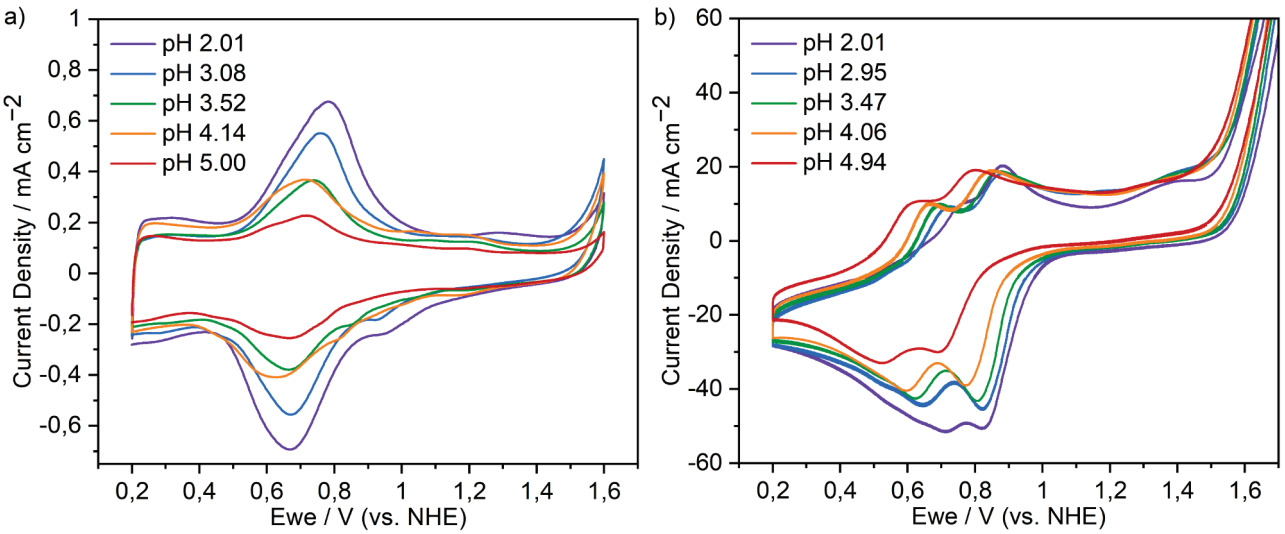

Fig. S16 Representative cyclic voltammograms of $[Ru(tpy)(pic\text{-}PO_3H_2)(H_2O)]^+(Cl)^-$ used for the construction of the Pourbaix diagrams. a) Immobilised on a *meso*-ITO electrode. b) Homogeneous solution.

Crystal data

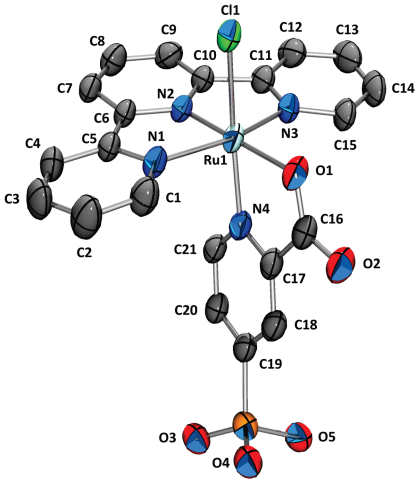

Fig. S17 Displacement ellipsoids of [Ru(tpy)(pic-PO_3H_2)Cl]. Hydrogen atoms have been omitted for clarity; thermal ellipsoids represent 50% probability. Single crystals were obtained through vapor diffusion (MeOH/THF).

Experimental

Single-crystal X-ray diffraction data were collected at 160(1) K on a *Rigaku OD XtaLAB Synergy*, *Dualflex*, *Pilatus* 200K diffractometer using a single wavelength X-ray source (Cu Kα radiation: λ = 1.54184 Å) from a micro-focus sealed X-ray tube and an *Oxford* liquid-nitrogen *Cryostream* cooler. The selected suitable single crystal was mounted using polybutene oil on a flexible loop fixed on a goniometer head and immediately transferred to the diffractometer. Pre-experiment, data collection, data reduction and analytical absorption correction[7] were performed with the program suite *CrysAlisPro*.[8] Using *Olex*[8,9] the structure was solved with the *SHELXT*[10] small molecule structure solution program and refined with the *SHELXL2018/3* program package[11] by full-matrix least-squares minimization on F^2. *PLATON*[12] was used to check the result of the X-ray analysis. For more details about the data collection and refinement parameters, see the CIF file.

Table S2. Crystal data and structure refinement.

Empirical formula	C21H16ClN4O5PRu
Formula weight	571.87
Temperature/K	160(1)
Crystal system	monoclinic
Space group	C2/c
a/Å	14.06525(17)
b/Å	25.1567(4)
c/Å	13.9309(2)
α/°	90
β/°	100.0515(14)
γ/°	90
Volume/Å3	4853.58(13)
Z	8
ρcalc/g cm−3	1.565
μ/mm−1	7.208
F(000)	2288.0
Crystal size/mm3	0.17 × 0.015 × 0.015
Crystal description	dark red needles
Radiation	Cu Kα (λ = 1.54184)
2θ range for data collection/°	7.028 to 148.996
Index ranges	−17 ≤ h ≤ 17, −23 ≤ k ≤ 31, −16 ≤ l≤ 17
Reflections collected	24717
Independent reflections	4949 [Rint = 0.0522, Rsigma =0.0404]

Data/restraints/parameters	4949/0/304
Goodness-of-fit on F2	1.043
Final R indexes [I>=2σ (I)]	R1 = 0.0518, wR2 = 0.1359
Final R indexes [all data]	R1 = 0.0623, wR2 = 0.1444
Largest diff. peak/hole / e Å−3	2.40/−0.60

Table S3. Fractional atomic coordinates (×10^4) and equivalent Isotropic displacement parameters (Å^2×10^3) for **3**. U_{eq} is defined as 1/3 of of the trace of the orthogonalised U_{IJ} tensor.

Atom	**x**	**y**	**z**	**U(eq)**
C6	4011(3)	5050.0(17)	3771(3)	41.3(8)
C7	4541(3)	4610.6(19)	3592(3)	46.9(9)
C8	4080(3)	4121(2)	3429(4)	54.4(11)
C9	3106(3)	4074.0(19)	3472(3)	51.6(10)
C10	2598(3)	4514.4(17)	3658(3)	42.8(9)
C11	1563(3)	4554.3(19)	3732(3)	45.3(9)
C12	942(3)	4123(2)	3635(4)	55.0(11)
C13	−23(3)	4198(3)	3688(4)	62.5(14)
C14	−349(3)	4703(2)	3797(4)	61.0(13)
C15	294(3)	5119(2)	3908(3)	52.7(11)
C16	1279(3)	6583.4(19)	3934(3)	48.3(10)
C17	1519(3)	6454.4(18)	2957(3)	45.0(9)
C18	1317(3)	6787.6(19)	2163(3)	48.6(10)
C19	1549(3)	6634.8(18)	1286(3)	46.1(9)
C20	1945(3)	6134.3(18)	1213(3)	46.1(9)
C21	2143(3)	5814.6(17)	2038(3)	43.3(9)
Cl1	2795.8(7)	5289.9(5)	5834.9(8)	49.3(3)
N1	3683(2)	5932.7(15)	4247(3)	44.7(8)
N2	3047(2)	4996.0(15)	3794(2)	40.5(7)
N3	1252(2)	5049.0(16)	3918(3)	45.3(8)
N4	1948(2)	5971.2(14)	2902(3)	41.8(7)
O1	1554(2)	6249.0(13)	4604(2)	50.4(7)
O2	812(2)	6999.6(14)	4022(3)	56.1(8)
O3	1991(2)	6924.6(13)	−458(3)	54.9(8)
O4	1482(3)	7635.1(14)	654(3)	57.9(8)
O5	266(2)	7009.9(14)	−242(3)	56.3(8)
P1	1331.5(8)	7070.8(5)	232.1(9)	49.1(3)
Ru1	2346.4(2)	5594.8(2)	4187.9(2)	40.79(14)

Table S4. Anisotropic displacement parameters (Å^2×10^3) for **3**. The anisotropic displacement factor exponent takes the form: $-2\pi^2[h^2a\cdot 2U_{11}+2hka\cdot b\cdot U_{12}+\ldots]$.

Atom	**U_{11}**	**U_{22}**	**U_{33}**	**U_{23}**	**U_{13}**	**U_{12}**
C1	40(2)	53(3)	77(3)	−7(2)	−1(2)	−2.7(19)
C2	45(3)	53(3)	118(5)	−4(3)	2(3)	−11(2)
C3	33(2)	66(3)	101(4)	5(3)	6(2)	−13(2)
C4	29.5(19)	64(3)	68(3)	4(2)	6.2(19)	1.1(19)
C5	27.1(18)	55(2)	47(2)	4.1(18)	1.3(16)	3.5(16)
C6	26.4(16)	51(2)	45(2)	4.5(17)	0.9(15)	4.9(15)
C7	31.5(18)	62(3)	46(2)	4(2)	3.8(16)	9.3(18)
C8	46(2)	51(3)	64(3)	−2(2)	4(2)	10.3(19)
C9	49(2)	48(2)	54(2)	6(2)	−1.0(19)	0.9(19)

Atom	U_{11}	U_{22}	U_{33}	U_{23}	U_{13}	U_{12}
C10	31.1(19)	51(2)	44(2)	5.4(17)	0.3(16)	0.2(16)
C11	31.9(19)	57(2)	44(2)	3.4(19)	−2.9(16)	−3.7(17)
C12	44(2)	63(3)	53(3)	7(2)	−5.5(19)	−9(2)
C13	40(2)	86(4)	56(3)	9(3)	−8(2)	−22(2)
C14	27.5(19)	93(4)	60(3)	1(3)	0.4(18)	−8(2)
C15	25.1(17)	77(3)	53(2)	6(2)	−1.3(16)	1.6(19)
C16	31.9(18)	56(2)	56(3)	1(2)	3.1(17)	6.5(17)
C17	28.5(17)	49(2)	56(2)	0.8(19)	4.7(16)	4.3(16)
C18	33.7(19)	49(2)	60(3)	4(2)	2.1(18)	3.5(17)
C19	31.4(18)	48(2)	57(2)	6.3(19)	3.6(17)	1.2(16)
C20	32.8(18)	52(2)	52(2)	−1.3(19)	3.2(16)	2.5(17)
C21	30.4(18)	44(2)	53(2)	1.4(18)	0.4(16)	3.1(16)
Cl1	28.4(4)	64.6(7)	52.8(6)	6.6(5)	1.2(4)	2.2(4)
N1	27.8(15)	48.7(19)	55(2)	−0.9(16)	−0.9(14)	2.9(13)
N2	25.9(14)	51.4(19)	41.8(17)	6.1(14)	−0.7(12)	3.6(13)
N3	24.5(14)	60(2)	50(2)	6.3(16)	1.8(13)	−0.2(14)
N4	27.2(14)	46.3(18)	50.2(19)	1.6(15)	1.6(13)	2.8(13)
O1	36.9(14)	58.6(18)	54.4(18)	−0.8(14)	4.4(13)	15.4(13)
O2	45.8(17)	57.7(19)	65(2)	0.2(15)	10.0(15)	16.8(14)
O3	47.7(17)	52.9(18)	66(2)	2.1(15)	13.9(15)	−9.1(14)
O4	47.9(18)	51.2(18)	77(2)	5.6(16)	18.9(17)	−3.0(14)
O5	41.7(16)	60.1(19)	65(2)	14.7(16)	4.6(14)	−7.4(14)
P1	39.9(5)	48.3(6)	59.5(7)	6.7(5)	9.9(5)	−4.2(4)
Ru1	22.86(18)	48.1(2)	49.2(2)	3.03(13)	0.27(12)	4.74(11)

Table S5. Bond lengths for **3**.

Atom	Atom	Length/Å	Atom	Atom	Length/Å
C1	C2	1.382(7)	C16	C17	1.495(6)
C1	N1	1.345(6)	C16	O1	1.265(5)
C2	C3	1.382(8)	C16	O2	1.253(5)
C3	C4	1.370(8)	C17	C18	1.377(6)
C4	C5	1.391(6)	C17	N4	1.365(5)
C5	C6	1.452(6)	C18	C19	1.373(7)
C5	N1	1.376(5)	C19	C20	1.388(6)
C6	C7	1.380(6)	C19	P1	1.815(5)
C6	N2	1.369(5)	C20	C21	1.391(6)
C7	C8	1.391(7)	C21	N4	1.341(6)
C8	C9	1.387(7)	Cl1	Ru1	2.3970(11)
C9	C10	1.367(7)	N1	Ru1	2.052(3)
C10	C11	1.481(6)	N2	Ru1	1.931(4)
C10	N2	1.364(6)	N3	Ru1	2.048(4)
C11	C12	1.385(7)	N4	Ru1	2.017(4)
C11	N3	1.359(6)	O1	Ru1	2.124(3)
C12	C13	1.384(7)	O3	P1	1.494(3)
C13	C14	1.368(9)	O4	P1	1.537(4)
C14	C15	1.374(7)	O5	P1	1.536(3)
C15	N3	1.356(5)			

Table S6. Bond angles for **3**.

Atom	Atom	Atom	Angle/°	Atom	Atom	Atom	Angle/°
N1	C1	C2	121.9(5)	C1	N1	C5	119.1(4)
C3	C2	C1	119.2(5)	C1	N1	Ru1	127.5(3)
C4	C3	C2	119.8(4)	C5	N1	Ru1	113.2(3)
C3	C4	C5	119.5(5)	C6	N2	Ru1	119.1(3)
C4	C5	C6	124.4(4)	C10	N2	C6	121.4(4)
N1	C5	C4	120.6(4)	C10	N2	Ru1	119.0(3)
N1	C5	C6	115.0(3)	C11	N3	Ru1	113.1(3)
C7	C6	C5	128.0(4)	C15	N3	C11	118.0(4)
N2	C6	C5	112.4(4)	C15	N3	Ru1	129.0(3)
N2	C6	C7	119.5(4)	C17	N4	Ru1	115.2(3)
C6	C7	C8	119.2(4)	C21	N4	C17	118.2(4)
C9	C8	C7	120.3(4)	C21	N4	Ru1	126.2(3)
C10	C9	C8	119.4(4)	C16	O1	Ru1	114.9(3)
C9	C10	C11	128.3(4)	O3	P1	C19	109.6(2)
N2	C10	C9	120.1(4)	O3	P1	O4	114.47(19)
N2	C10	C11	111.5(4)	O3	P1	O5	111.6(2)
C12	C11	C10	123.5(4)	O4	P1	C19	104.8(2)
N3	C11	C10	115.4(4)	O5	P1	C19	107.52(18)
N3	C11	C12	121.2(4)	O5	P1	O4	108.4(2)
C13	C12	C11	119.6(5)	N1	Ru1	Cl1	90.41(10)
C14	C13	C12	119.0(5)	N1	Ru1	O1	100.90(13)
C13	C14	C15	119.4(4)	N2	Ru1	Cl1	87.70(10)
N3	C15	C14	122.4(5)	N2	Ru1	N1	79.93(14)
O1	C16	C17	116.0(4)	N2	Ru1	N3	80.19(14)
O2	C16	C17	118.4(4)	N2	Ru1	N4	100.99(14)
O2	C16	O1	125.5(4)	N2	Ru1	O1	178.98(13)
C18	C17	C16	123.5(4)	N3	Ru1	Cl1	91.46(10)
N4	C17	C16	114.6(4)	N3	Ru1	N1	159.93(15)
N4	C17	C18	121.9(4)	N3	Ru1	O1	98.96(14)
C19	C18	C17	119.8(4)	N4	Ru1	Cl1	170.45(11)
C18	C19	C20	118.7(4)	N4	Ru1	N1	87.26(14)
C18	C19	P1	121.2(3)	N4	Ru1	N3	93.90(14)
C20	C19	P1	120.1(4)	N4	Ru1	O1	78.49(13)
C19	C20	C21	119.2(4)	O1	Ru1	Cl1	92.87(9)
N4	C21	C20	122.0(4)				

Table S7. Hydrogen bonds for **3**.

D	H	A	d(D–H)/Å	d(H–A)/Å	d(D–A)/Å	D–H–A/°
C2	H2	O4[1]	0.95	2.60	3.248(6)	125.9
C12	H12	O3[2]	0.95	2.42	3.173(6)	136.3
O4	H4A	O3[3]	0.90(8)	1.58(8)	2.473(5)	174(7)

[1]1/2+X,3/2−Y,1/2+Z; [2]+X,1−Y,1/2+Z; [3]1/2−X,3/2−Y, −Z

Table S8. Torsion angles for **3**.

A	B	C	D	Angle/°	A	B	C	D	Angle/°
C1	C2	C3	C4	1.8(10)	C14	C15	N3	C11	5.4(7)
C2	C1	N1	C5	1.7(8)	C14	C15	N3	Ru1	−174.2(4)
C2	C1	N1	Ru1	−172.6(4)	C16	C17	C18	C19	−178.9(4)
C2	C3	C4	C5	−0.4(9)	C16	C17	N4	C21	176.8(3)
C3	C4	C5	C6	179.2(5)	C16	C17	N4	Ru1	−9.2(4)
C3	C4	C5	N1	−0.5(7)	C17	C16	O1	Ru1	2.4(5)
C4	C5	C6	C7	8.3(7)	C17	C18	C19	C20	2.7(6)
C4	C5	C6	N2	−173.1(4)	C17	C18	C19	P1	−178.0(3)
C4	C5	N1	C1	−0.1(7)	C18	C17	N4	C21	−2.3(6)
C4	C5	N1	Ru1	175.0(4)	C18	C17	N4	Ru1	171.7(3)
C5	C6	C7	C8	179.0(4)	C18	C19	C20	C21	−3.3(6)
C5	C6	N2	C10	−177.7(4)	C18	C19	P1	O3	156.3(3)
C5	C6	N2	Ru1	−5.5(5)	C18	C19	P1	O4	33.0(4)
C6	C5	N1	C1	−179.9(4)	C18	C19	P1	O5	−82.2(4)
C6	C5	N1	Ru1	−4.8(5)	C19	C20	C21	N4	1.1(6)
C6	C7	C8	C9	−1.6(7)	C20	C19	P1	O3	−24.4(4)
C7	C6	N2	C10	1.0(6)	C20	C19	P1	O4	−147.7(3)
C7	C6	N2	Ru1	173.2(3)	C20	C19	P1	O5	97.1(4)
C7	C8	C9	C10	1.2(7)	C20	C21	N4	C17	1.7(6)
C8	C9	C10	C11	179.8(4)	C20	C21	N4	Ru1	−171.6(3)
C8	C9	C10	N2	0.3(7)	N1	C1	C2	C3	−2.5(9)
C9	C10	C11	C12	1.3(7)	N1	C5	C6	C7	−172.0(4)
C9	C10	C11	N3	−179.6(4)	N1	C5	C6	N2	6.6(5)
C9	C10	N2	C6	−1.5(6)	N2	C6	C7	C8	0.5(6)
C9	C10	N2	Ru1	−173.6(3)	N2	C10	C11	C12	−179.2(4)
C10	C11	C12	C13	−178.2(4)	N2	C10	C11	N3	0.0(5)
C10	C11	N3	C15	174.3(4)	N3	C11	C12	C13	2.7(7)
C10	C11	N3	Ru1	−6.1(5)	N4	C17	C18	C19	0.1(6)
C11	C10	N2	C6	179.0(4)	O1	C16	C17	C18	−176.6(4)
C11	C10	N2	Ru1	6.8(5)	O1	C16	C17	N4	4.3(6)
C11	C12	C13	C14	2.6(7)	O2	C16	C17	C18	4.9(7)
C12	C11	N3	C15	−6.6(6)	O2	C16	C17	N4	−174.1(4)
C12	C11	N3	Ru1	173.1(3)	O2	C16	O1	Ru1	−179.3(4)
C12	C13	C14	C15	−3.8(7)	P1	C19	C20	C21	177.4(3)
C13	C14	C15	N3	−0.2(7)					

Table S9. Hydrogen atom coordinates (Å×10^4) and isotropic displacement parameters (Å^2×10^3) for **3**.

Atom	x	y	z	U(eq)
H1	3480.83	6675.89	4652.76	69
H2	4989.09	6998.74	4475.83	88
H3	6138.99	6413.93	4048.24	81
H4	5730.33	5529.75	3712.08	65
H7	5211.54	4641.93	3578.97	56
H8	4434.44	3818.17	3288.41	65
H9	2794.26	3738.47	3374.03	62
H12	1176.04	3776.98	3532.97	66
H13	−451.06	3904.1	3649.83	75
H14	−1015.72	4765.8	3796.42	73

Atom	x	y	z	U(eq)
H15	59.59	5467.98	3980.75	63
H18	1019.51	7122.08	2221.83	58
H20	2080.2	6011.5	605.55	55
H21	2424.91	5474.88	1987.25	52
H4A	2050(60)	7770(30)	580(50)	87
H5	−230(50)	7080(30)	240(50)	84

Crystal Data for $C_{21}H_{16}ClN_4O_5PRu$ (*M* =571.87 g/mol): monoclinic, space group C2/c (no. 15), a = 14.06525(17) Å, b = 25.1567(4) Å, c = 13.9309(2) Å, β = 100.0515(14)°, V = 4853.58(13) Å^3, Z = 8, T = 160(1) K, μ(Cu Kα) = 7.208 mm^{-1}, Dcalc = 1.565 g/cm^3, 24717 reflections measured (7.028° ≤ 2θ ≤ 148.996°), 4949 unique (R_{int} = 0.0522, R_{sigma} = 0.0404) which were used in all calculations. The final R_1 was 0.0518 (I > 2σ(I)) and wR_2 was 0.1444 (all data).

Refinement model description
Number of restraints - 0, number of constraints - unknown.
Details:
1. Fixed Uiso
   At 1.2 times of: All C(H) groups
   At 1.5 times of: All O(H) groups
2. Aromatic/amide H refined with riding coordinates:
   C1(H1), C2(H2), C3(H3), C4(H4), C7(H7), C8(H8), C9(H9), C12(H12), C13(H13), C14(H14), C15(H15), C18(H18), C20(H20), C21(H21)

NMR spectra of isolated compounds

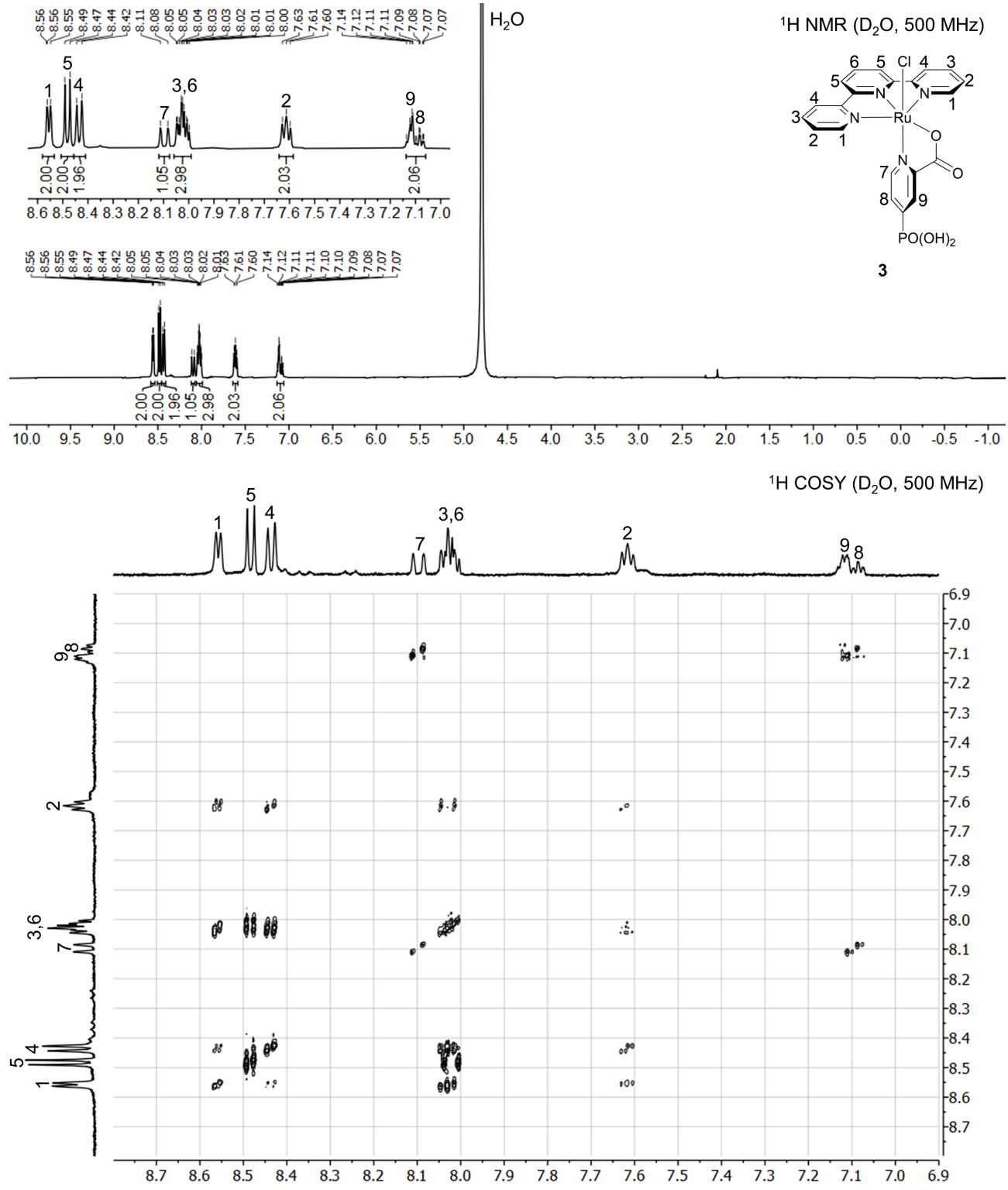

Fig. S18 ^{1}H NMR and ^{1}H COSY NMR of [Ru(tpy)(pic-PO_3H_2)Cl] (**3**) in D_2O.

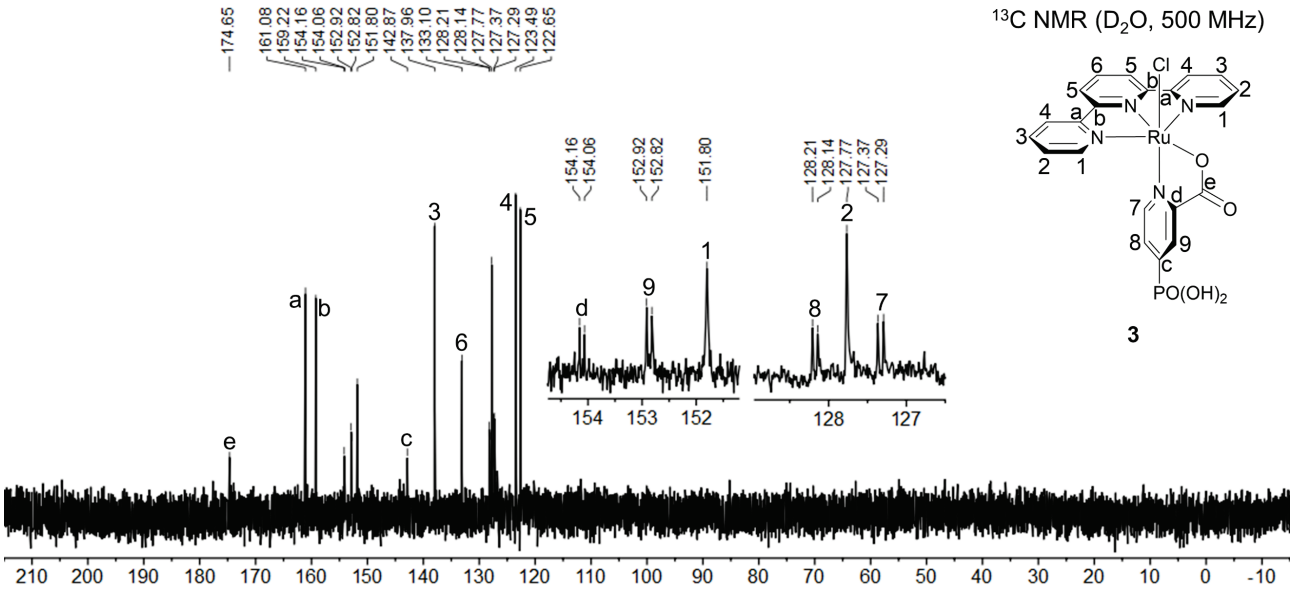

Fig. S19 ^{13}C NMR of [Ru(tpy)(pic-PO_3H_2)Cl] (**3**) in D_2O.

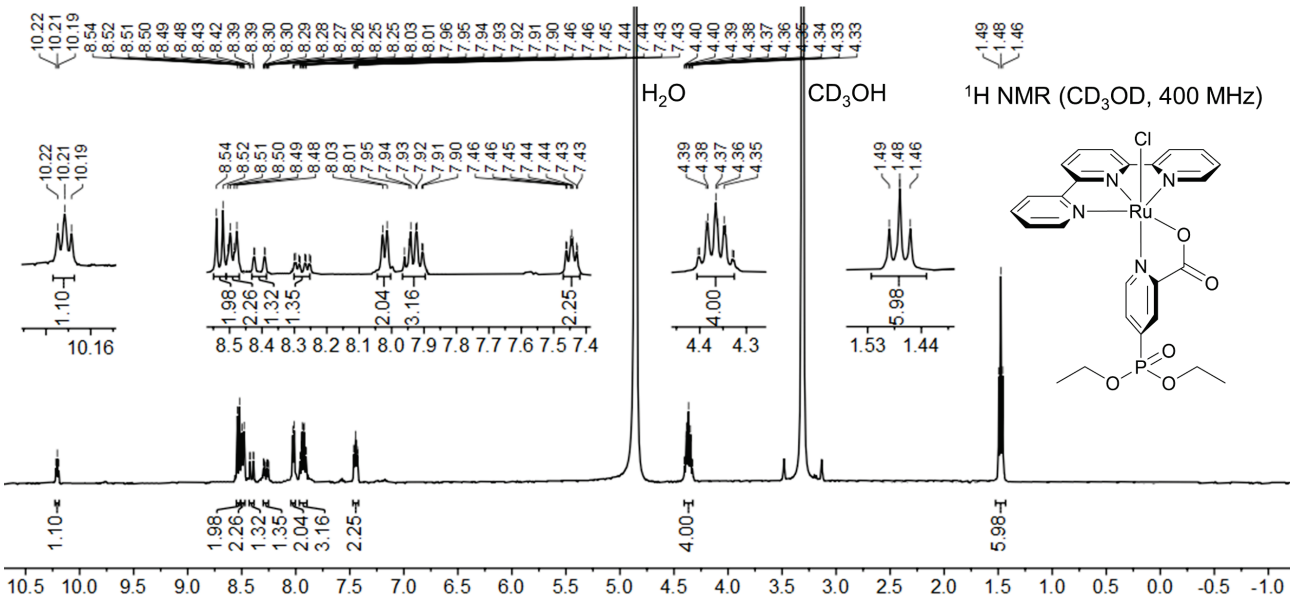

Fig. S20 ^{1}H NMR of [Ru(tpy)(pic-PO_3Et_2)Cl] in CD_3OD.

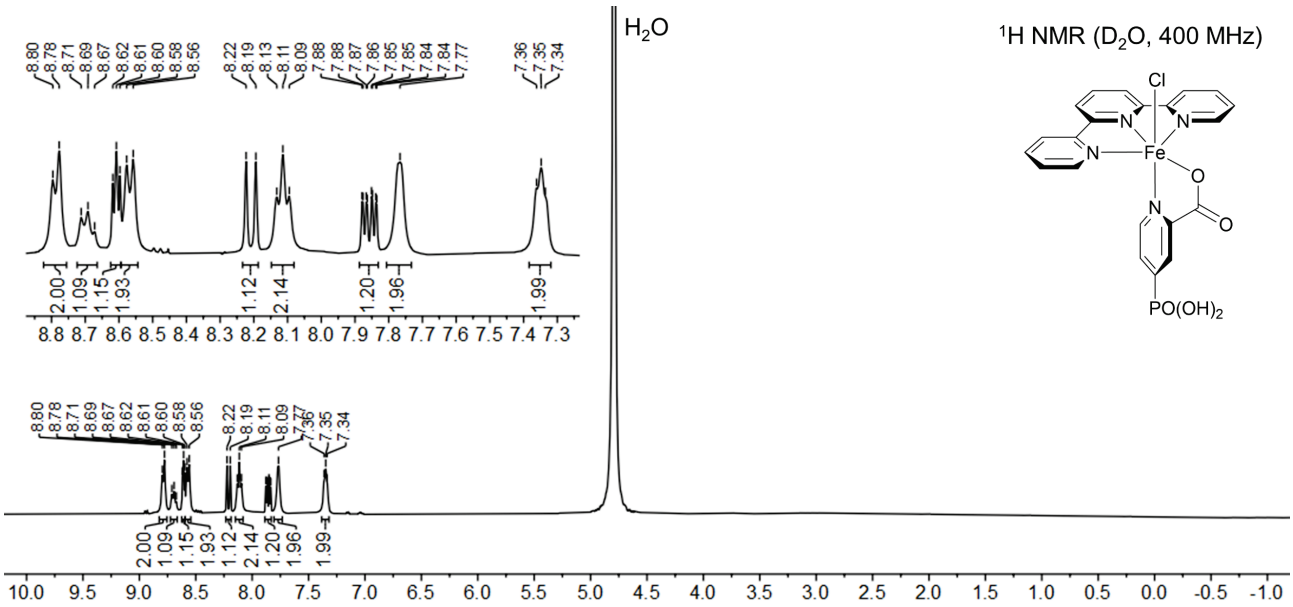

Fig. S21 ^{1}H NMR of [Fe(tpy)(pic-PO_3H_2)Cl] in D_2O.

References

1 B. P. Sullivan, J. M. Calvert and T. J. Meyer, *Inorg. Chem.*, 1980, **19**, 1404–1407.
2 Z. A. Dziuganowska, K. Ślepokura, J.-N. Volle, D. Virieux, J.-L. Pirat and P. Kafarski, *J. Org. Chem.*, 2016, **81**, 4947–4954.
3 C. Costentin, G. Passard and J.-M. Savéant, *J. Am. Chem. Soc.*, 2015, **137**, 5461–5467.
4 E. S. Rountree, B. D. McCarthy, T. T. Eisenhart and J. L. Dempsey, *Inorg. Chem.*, 2014, **53**, 9983–10002.
5 F. G. Bordwell, J. Pei. Cheng and J. A. Harrelson, *J. Am. Chem. Soc.*, 1988, **110**, 1229–1231.
6 J. J. Warren, T. A. Tronic and J. M. Mayer, *Chem. Rev.*, 2010, **110**, 6961–7001.
7 R. C. Clark and J. S. Reid, *Acta Crystallogr. Sect. A*, 1995, **51**, 887–897.
8 *CrysAlisPro*, version 1.171.40.68a, Rigaku Oxford Diffraction Ltd., Yarnton, Oxfordshire, England, 2019.
9 O. V. Dolomanov, L. J. Bourhis, R. J. Gildea, J. A. K. Howard and H. Puschmann, *J. Appl. Crystallogr.*, 2009, **42**, 339–341.
10 G. M. Sheldrick, *Acta Crystallogr. Sect. A*, 2015, **71**, 3–8.
11 G. M. Sheldrick, *Acta Crystallogr. Sect. C*, 2015, **71**, 3–8.
12 A. L. Spek, *Acta Crystallogr. Sect. D*, 2009, **65**, 148–155.